nature COMMUNICATIONS

ARTICLE

Received 17 April 2014 | Accepted 4 July 2014 | Published 8 August 2014

DOI: 10.1038/ncomms5596 OPEN

Aggregation-induced emission dots with high fluorescence quantum yield and high singlet oxygen generation for cancer-targeted photodynamic therapy in vivo

Jiechao Ge[1,*], Minghua Lan[1,*], Bingguang Zhou[1], Weiping Liu[1], Linggang Guo[1], Haiwang Wang[1], Qingguang Jia[1], Guangge Niu[1], Xingguang Huang[1], Hongguang Zhang[1], Xiaoguang Meng[1], Peifeng Wu[1], Chun-Sing Lee[2], Wenjun Zhang[2] & Xiaodong Hang[3]

Conventional photodynamic therapy (PDT) agents are affected by the low singlet oxygen ($^1O_2$) generation, and the hydrophobic photosensitizers. Here we report aggregation-induced emission dots (AIE dots) with high $^1O_2$ generation ability for efficient PDT agents. The AIE dots are prepared from amphiphilic polymers containing AIE photosensitizers. The fluorescence quantum yield of AIE dots can be as high as ~13%, which is 13 times brighter than the commercial PDT agents. The AIE dots are excited by the UV light and the blue light, and the emission wavelength can be tuned from green to near-infrared. Through *in vitro* and *in vivo* studies, we demonstrate that AIE dots can be used as PDT agents, and the AIE dots with high fluorescence quantum yield and high $^1O_2$ generation ability can ablate cancer cells or tumors efficiently. The results open a door for fabrication of bright and photostable organic nanoparticles with high $^1O_2$ generation ability for image-guided PDT of deep-seated cancers.

[1] Key Laboratory of Photochemical Conversion and Optoelectronic Materials, Technical Institute of Physics and Chemistry (TIPC), Chinese Academy of Sciences, Beijing 100190, China. [2] Center of Super-Diamond and Advanced Films (COSDAF) and Department of Physics and Materials Science, City University of Hong Kong, Hong Kong SAR 999077, China. [3] Institute of Microstructure and Properties of Advanced Materials, Beijing University of Technology, Beijing 100124, China. * These authors contributed equally to this work. Correspondence and requests for materials should be addressed to P.W. (email: wangpf@mail.ipc.ac.cn) or to W.Z. (email: apwjzh@cityu.edu.hk).

Owing to the high mortality rate caused by malignant tumours, much effort has been devoted to identify an efficient approach to treat cancer[1]. Among the emerging cancer therapy methods, photodynamic therapy (PDT) surpasses the traditional methods (surgery, chemotherapy and radiotherapy) because it is noninvasive in nature, has fewer side effects, causes negligible drug resistance and has low systemic toxicity[2–4]. In PDT, cancerous cells are locally killed by reactive oxygen species (ROS) such as $^1O_2$ produced by a photosensitizer (PS) under illumination and in the presence of oxygen[2]. Activatable photosensitizers, such as porphyrin, phthalocyanines and bacteriochlorin derivatives, have been demonstrated to possess simultaneous cancer imaging and therapy capabilities, and some of these photosensitizers have been approved for clinical use[5]. However, the current applications are often limited by the drawbacks of these organic PDT agents, including poor water dispersibility, photostability and their inability to be absorbed in the region (>700 nm) where the skin is most transparent[6,7]. Although the alternative semiconductor quantum dots (QDs) are superior to organic photosensitizers in terms of photostability and water dispersability[8–10], the clinical translation of these agents has been impeded owing to their cytotoxicity and low ROS-generation efficiency[11–15]. Therefore, approaches such as modifying semiconductor QDs with a traditional PDT agent (porphyrin derivative, Ce6) and then coating them with a shell of peptides have been developed to reduce the cytotoxicity of these agents[16]. A PDT agent with a high $^1O_2$ quantum yield and excellent photostability and biocompatibility is highly desirable.

Carbon nanostructures have a wide variety of promising applications in environmental, energy and biomedical fields[17–21]. In particular, the photoluminescence (PL) effect of carbon QDs (CQDs) enables them to be extensively applied in bioimaging and biosensing[22–25]. Green-light-emitting CQDs have been conjugated to Ce6 to improve their biocompatibility and light-emission intensity[26]. This composite allowed simultaneous imaging and *in vivo* PDT of tumours, however, the PDT efficiency was dominated by Ce6. Very recently, it was reported that graphene quantum dot (GQDs) passivated with polyethylene glycol derivatives could generate $^1O_2$ upon irradiation with blue light[27]. However, the system exhibited only limited *in vitro* PDT efficiency owing to a low $^1O_2$ quantum yield.

In this study, we prepare highly water-dispersible GQDs in large quantities using a hydrothermal method with polythiophene derivatives (PT2) as the carbon source[28]. The GQDs exhibit a broad absorption in the UV-visible region and a strong emission peaking at 680 nm. We demonstrate that the GQDs exhibit good biocompatibility and excellent $^1O_2$ generation capability with a quantum yield of ~1.3. Moreover, *in vitro* and *in vivo* studies suggest that the GQDs can be applied as a PDT agent for the simultaneous imaging and highly efficient treatment of cancer.

Results

Structure and composition of GQDs. To investigate the intrinsic crystal structure of GQDs, scanning transmission electron microscopy (STEM) was performed. Figure 1a presents a STEM image of the GQDs, with diameters ranging from 2 to 6 nm. The high-resolution TEM (HRTEM) observation of the GQDs in Fig. 1b reveals the crystallinity of the GQDs; the labelled interplanar distance of 0.21 nm agrees with the (100) lattice spacing of graphene along the [001] direction, and that of 0.31 nm corresponds to the lattice fringes of (002) planes[29,30]. A typical X-ray diffraction pattern and a Raman spectrum (Supplementary Fig. 1) further verify the sp^2 configuration of the GQDs[31,32]. X-ray photoelectron spectroscopy (XPS) measurements were performed to probe the composition of the GQDs. The survey spectrum in

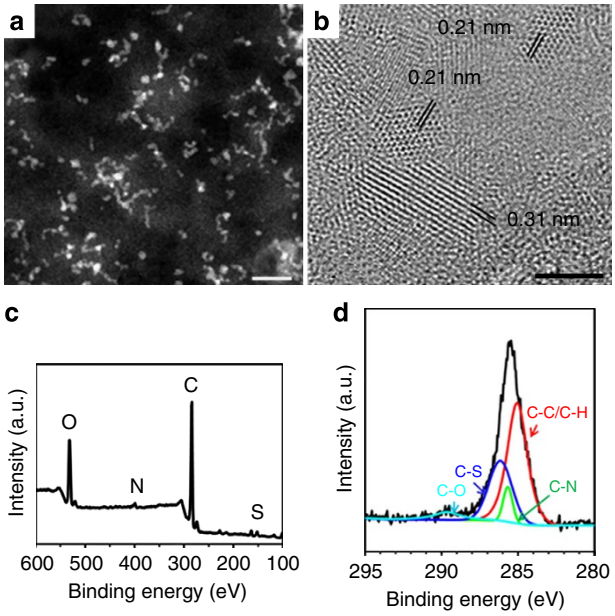

Figure 1 | Characterization of GQDs. (**a**) TEM age . Sca e ba., 20 . (**b**) HRTEM age . Sca e ba., 2 . (**c**) XPS . e ec. . (**d**) Dec f h gh-. e . C1 XPS ec. a.

Fig. 1b indicates the presence of carbon, nitrogen, sulphur and oxygen; deconvolution of the high-resolution C1s XPS spectra (Fig. 1c) reveals peaks at 285.0, 285.7, 286.2 and 289.7 eV, corresponding to C–C, C–N, C–S and C–O bonding, respectively. The nitrogen and sulphur content were evaluated to be 1.6% and 5.8%, respectively (Supplementary Fig. 2a). The high-resolution N1s and S2p spectra in Supplementary Fig. 2b,c also support the formation of C–N and C–S bonding, which implies the incorporation of nitrogen and sulphur into the GQDs. Moreover, oxygen is physically and chemically adsorbed on the GQDs (Supplementary Fig. 2d,e).

Photophysical and photochemical properties of GQDs. Figure 2a presents the UV–vis absorption and PL spectra of the GQDs, illustrating that the GQDs have a broad absorption, from 400 to 700 nm, and a deep-red emission peaking at 680 nm. The GQDs exhibited a large Stokes shift of 205 nm, implying that the self-absorption of their emission and the measurement interference between excitation light and scattered light could be minimized. To further understand the luminescence properties, the time-resolved PL spectra of GQD aqueous solution were measured with an excitation of 488 nm. Analysis of the fluorescence decay kinetics revealed three exponential decays, with the longest lifetime being 7.52 ns (Fig. 2b); a lifetime on the ns level suggests the singlet state nature of the GQD emission. The fluorescence quantum yield of the GQDs was measured to be 0.054 in an O_2 atmosphere using a spectrometer attached to an integrating sphere. Both the fluorescence lifetime and fluorescence quantum yield of the GQDs increased when the measurements were performed in an air or N_2 atmosphere. A similar tendency was also observed in 9,10-dicyanoanthracene, which contains a fused-ring aromatic with a large π-conjugated structure and enables $^1O_2$ generation from both singlet and triplet states (Supplementary Table 1)[33]. Furthermore, the GQDs exhibited superior photostability to CdTe QDs (conventional red-emitting semiconductor QDs) and protoporphyrin IX (PpIX, a classic photosensitizer; Fig. 2c and Supplementary Fig. 3) as well as good pH stability (Supplementary Fig. 4), which are essential for biomedical applications[34–36].

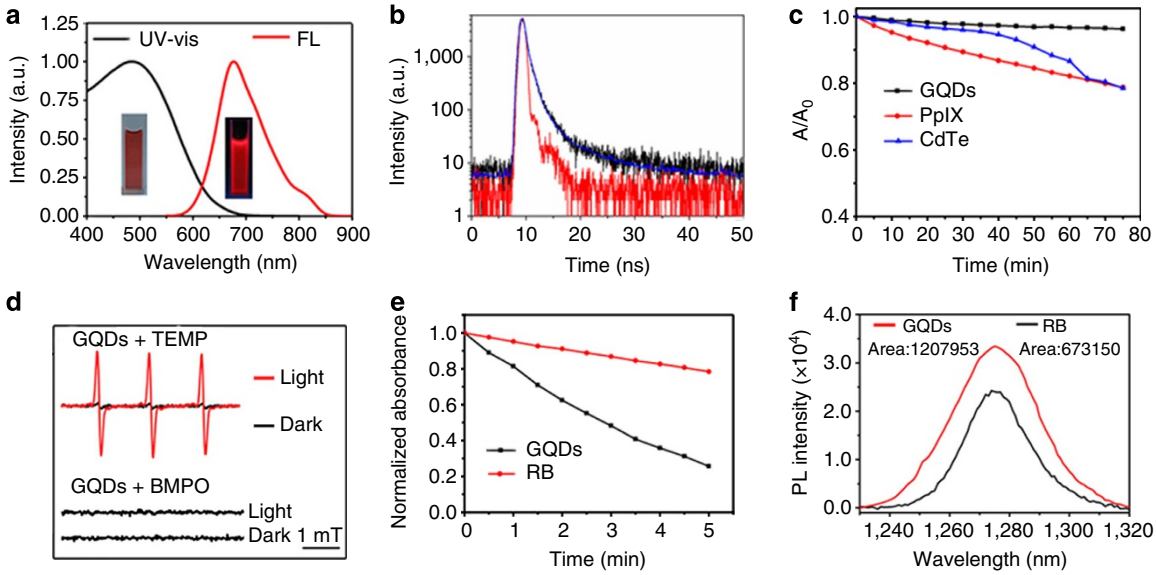

Figure 2 | Photophysical and photochemical properties of GQDs. (**a**) N a ed UV ab. b de ec. a (λ_e = 500) f he GQD d e. ed a.e a. e e.a. e. The e. h a h g a h d e ce ce age f he GQD de. UV gh. (365). (**b**) F e ce ce deca c e (b ac e) f GQD ec ded a. 680 h e c a. f 488 . Red e: he e; b e e: g f he e ce ce deca c e. F = A + B_1e $(-t/\tau_1)$ + B_2e $(-t/\tau_2)$ + B_3e $(-t/\tau_3$; τ_1 = 0.27 , τ_2 = 1.10 , τ_3 = 7.52). (**c**) A c a f he h ab e f he GQD , CdTe QD d P IX. A f he a e e.e c ad a.ed g a 500-W e a . A_0 d A a.e he ab b ce f he a e. a. 470 bef e d af.e ad a. , e ec e . Af.e 75 f ad a. b dec e a b e.ed he ab b ce f he GQD , h e he ab b ce f P IX d he CdTe QD dec ea ed be 78% f he a a e. (**d**) The ESR g a f $^1O_2$ ( ) d he ROS (d) b.d ed ad a. f GQD f 8 he e ce f 2,2,6,6-Te. a e.h e d e d 5-.e.-b ca.b 5- e.h -1- e *N*- de, e ec e . (**e**) The a ed ab b ce f Na_2-ADPA a. 378 a af c. f ad a. e he e ce f GQD d RB. (**f**) The $^1O_2$ e a. ~1,280 d ced b he GQD d RB a CH_3CN-D_2O e (/ = 15/1) de e c a. h a 532 a e..

The electron spin resonance (ESR) technique was employed to detect the ROS generation by the GQDs under irradiation. 2,2,6,6-Tetramethylpiperidine and 5-tert-butoxycarbonyl 5-methyl-1-pyrroline *N*-oxide were used as $^1O_2$ and $O_2^{-\bullet}$ (or $OH^\bullet$) trappers, respectively. As illustrated in Fig. 2d (top, red line) and Supplementary Fig. 5, a characteristic $^1O_2$-induced signal, 2,2,6,6-tetramethylpiperidine-1-oxyl, was observed in the ESR spectra only under irradiation, and its intensity increased with the increase in irradiation time. No other ROS signals were observed (Fig. 2d, bottom). These results verify that it is the energy transfer (ET), not the electron transfer, from the GQDs to oxygen that is responsible for the sensitization of ground-state oxygen[2]. To assess the ability of GQDs to generate $^1O_2$, the $^1O_2$ quantum yield was measured using a chemical trapping method with disodium 9,10-anthracen-dipropionic acid (Na_2-ADPA) as the trapping agent and Rose Bengal (RB) as the standard photosensitizer ($^1O_2$ quantum yield $\Phi_{RB} = 0.75$ in water)[14]. As illustrated in Fig. 2e, in the presence of GQDs or RB under irradiation with white light, the absorbance of the Na_2-ADPA solution at 378 nm, decreased gradually with prolonged irradiation time, indicating the degradation of Na_2-ADPA by $^1O_2$ generated by GQDs and RB[37]. Nevertheless, the degradation rate of Na_2-ADPA resulting from the GQDs was far larger than that from the RB. Thus, the $^1O_2$ quantum yield of the GQD solution was calculated to be 1.3 (Supplementary Fig. 6 and Supplementary Note 1). Moreover, measurements at different excitation wavelengths, 538, 549 and 562 nm, also revealed an almost consistent $^1O_2$ quantum yield of the GQDs of ~1.3 (Supplementary Fig. 7 and Supplementary Table 2).

By comparing the peak areas of $^1O_2$ emission at ~1,280 nm induced by the GQDs and RB in a CH_3CN-D_2O solution under excitation with a 532-nm laser, the GQD $^1O_2$ quantum yield was determined to be 1.34 based on the known value of $\Phi_{RB} = 0.76$ in CH_3CN, as depicted in Fig. 2f (refs 38,39). This result agrees very well with that obtained using the chemical trapping method above. Further investigation illustrated that the $^1O_2$ quantum yields were maintained at ~1.3 at pH values ranging from 6 to 8 (Supplementary Table 3). To the best of our knowledge, this efficiency is the highest $^1O_2$-generating efficiency ever reported for PDT agents and is approximately twice as high as that of all of the state-of-the-art PDT agents[6,12].

***In vitro* imaging and PDT**. These highly photostable, water-dispersible and red-emitting GQDs can be used as fluorescence-imaging agents. Staining HeLa cells with GQDs led to strong PL emission from the cells; the corresponding fluorescence image in Fig. 3a demonstrates that the GQDs labelled only the cytoplasm and not the nucleus, similar to the observations for other C-dots[40].

The photodynamic activity of the GQDs against cancer cells was investigated by monitoring the morphology variation of HeLa cells in the presence of GQDs using laser-scanning confocal microscopy. In these experiments, Hoechst 33342 was also added to stain the nucleus. As demonstrated in Fig. 3b, irradiation led to cell morphology changes, including the shrinkage of cells and the formation of numerous blebs. The corresponding fluorescence images in Fig. 3c and Supplementary Fig. 8 also confirm that photo-induced cell death was accompanied by nuclear condensation[41–42]. The process of cell death is also presented in two video files, which were recorded with bright-field and fluorescent microscopes (Supplementary Movies 1 and 2). In control experiments, the cells did not undergo obvious morphological changes in the absence of GQDs (Supplementary Fig. 9).

A standard 3-(4,5-dimethylthiazol-2-yl)-2,5-diphenyl-2H-tetrazolium hydrobromide (MTT) assay was performed to quantitatively evaluate the PDT efficiency and cytotoxicity of

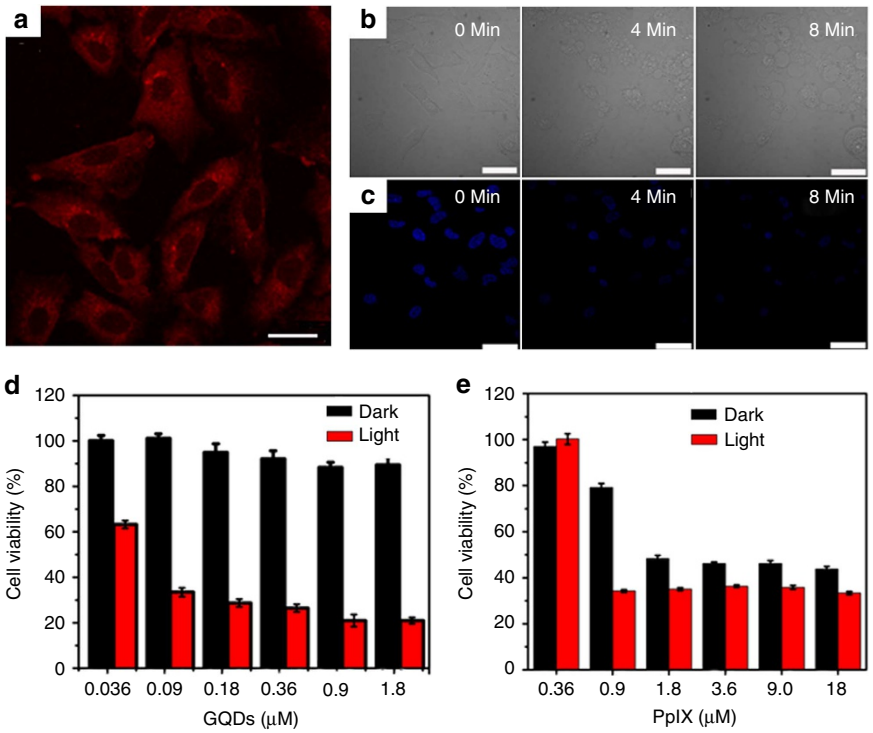

Figure 3 | *In vitro* imaging and PDT. (**a**) C f ca e ce c c age f HeLa ce abe ed h GQD (0.4 μM). Sca e ba, 20 μ . (**b**) T e-de e de c f ca b gh e d d (**c**) c e d g e ce ce age f HeLa ce c ba ed h GQD (0.4 μM) d H ech 33342 (1.8 μM) af e ad a h 405 d 633 a e . Sca e ba, 50 μ . D e-de e de PDT effec f he ce ab f HeLa ce : (**d**) GQD he c ce a ge 0.036 1.8 μM d (**e**) P IX he c ce a ge 0.36 18 μM.

the GQDs compared with the classic photosensitizer PpIX. In these experiments, HeLa cells were irradiated for a constant duration of 10 min in phosphate-buffered solution (PBS) with GQDs from 0.036 to 1.8 μM or PpIX from 0.36 to 18 μM, as illustrated in Fig. 3d,e, respectively. A cell viability of 60% was observed in the presence of 0.036 μM GQDs; this value decreased with increasing GQD concentration, decreasing to ~20% for the 1.8-μM GQD solution. However, GQDs have little effect on the survival of HeLa cells in the dark even at a concentration of 1.8 μM, indicating the low cytotoxicity and good biocompatibility of GQDs[23]. By contrast, a much smaller cell viability of 55% was obtained for the 1.8-μM PpIX solution in the dark condition, and more than 35% of the cells survived even upon irradiation (Fig. 3e). Further increasing the PpIX concentration did not induce an obvious change in cell viability. It was also observed that GQDs exhibit an even stronger PDT effect than PpIX at one-tenth the concentration. The above results verify that GQDs are superior to PpIX in terms of both their high PDT efficiency and low cytotoxicity.

***In vivo* imaging and PDT**. To investigate the *in vivo* fluorescence imaging capability of GQDs, 20 μl GQD aqueous solution (27 μM) was injected into the back of a nude mouse. As depicted in Fig. 4a,b, the injection sites showed a much higher fluorescence intensity than the background signal produced by the mouse skin, and a high signal-to-noise ratio of 229.5 was achieved (Supplementary Table 4). More importantly, no apparent fluorescence intensity decay was observed at the injection sites, and the injected GQDs did not show evidence of obvious diffusion, even 1 week after injection (Supplementary Fig. 10).

The performance of the GQDs for *in vivo* PDT was evaluated using female BALB/nu mice with subcutaneous breast cancer xenografts as an animal model. Three groups of MDA MB-231 green-fluorescent protein tumour-bearing mice with 5 mice per group were used. For the PDT group, mice were intratumorally injected with GQDs (dose = 4 mg kg^{-1}) and then irradiated twice, on the first and seventh days, for 10 min with white light (400–800 nm) at a power density of 80 mW cm^{-2}. The control groups included mice that received a GQD injection at the same dose but were not irradiated (the C1 group) and mice that did not received a GQD injection but were irradiated (the C2 group). The tumour sizes were measured using a caliper every other day. As illustrated in Fig. 4c, in the PDT group, the tumours first turned dark and festered, which increased the tumour size slightly. The tumours began to decompose after 9 days and were destroyed after 17 days, leaving black scars at the original sites, which fell off ~1 week later[43]. No tumour regrowth was observed in the PDT group over the course of 50 days. In contrast, the tumours in the C1 and C2 groups grew significantly during the study period (Fig. 4d) and exhibited strong green fluorescence (Supplementary Fig. 11), indicating that neither light irradiation nor GQD injection alone inhibited the tumour growth. Our experiments also ruled out the photothermal effect of GQDs in killing the tumour cells (Supplementary Fig. 12 and Supplementary Note 2). Moreover, the *in vivo* toxicity of the GQDs was also roughly estimated by monitoring the weight change of the mice in the study period, and no obvious side effects were revealed (Supplementary Fig. 13).

Discussion

In conventional PDT agents, such as porphyrin and phthalocyanines, $^1O_2$ is generated by ET from the excited triplet state (T_1) of the sensitizer to the ground-state oxygen ($^3O_2$), and the $^1O_2$ quantum yield is less than 1.0 (Fig. 5a, left). The extremely high $^1O_2$ quantum yield of the GQDs is considered to stem from a new $^1O_2$-generating mechanism, which can be termed multistate sensitization (MSS). According to the absorption and fluorescence spectra, the excited singlet state (S_1) energy of the GQDs was estimated to be ~49.3 kcal mol^{-1}, and the T_1 energy was

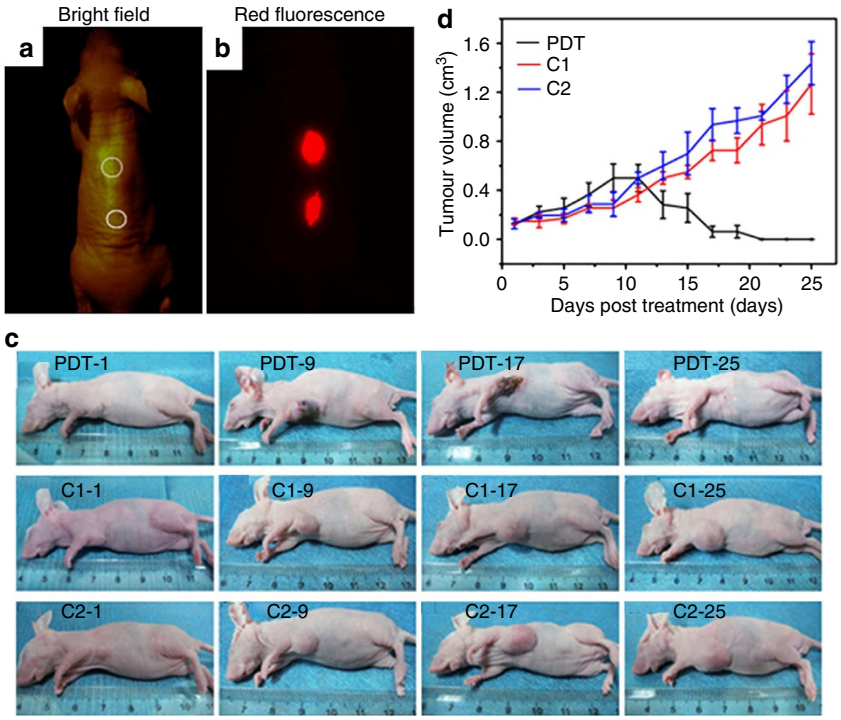

Figure 4 | *In vivo* imaging and PDT. (**a**) B gh - e d age a d (**b**) ed- e ce ce age af e bc e ec f GQD d ffe e a ea . The e c a a e g h a 502 540 , a d he c ec ed e ce ce cha e a 695 775 . (**c**) Ph g a h f ce af e a ea e he 1 ., 9 h, 17 h a d 25 h da . (PDT: GQD + gh ad a ; C1: GQD ; C2: gh ad a .) (**d**) T e-de e d g h c e (*n* = 5) af e d ffe e ea e . $P < 0.05$ f each g .

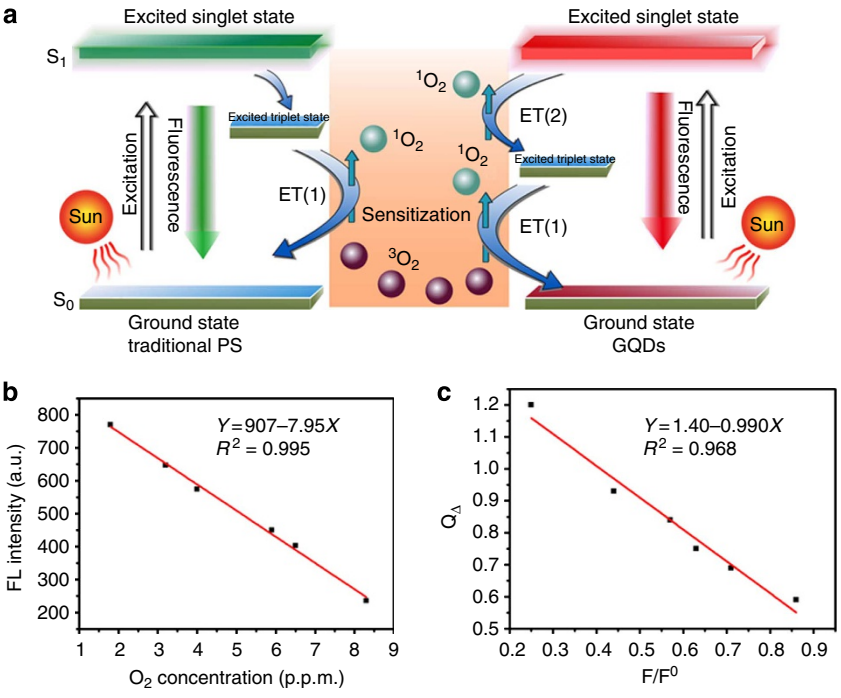

Figure 5 | Multistate sensitization mechanism. (**a**) Sche a c a f he $^1O_2$ g e a echa b c e a PDT age (ef) a d GQD (gh). (**b**) F e ce ce e f GQD a 680 e he O_2 c ce a . (**c**) The de e de ce f he $^1O_2$ a ed (Q_Δ) he e ce ce e a a 680 (F/F^0).

estimated to be between 22.5 and 26.5 kcal mol^{-1} above the ground state (G; Supplementary Fig. 14 and Supplementary Note 3). The energy gap (ΔE_{ST}) between S_1 and T_1 was thus calculated to be ~22.8 ~26.8 kcal mol^{-1}. In this case, both ΔE_{ST} and ΔE_{TG} (the energy gap between T_1 and G) are larger than the formation energy of $^1O_2$ (22.5 kcal mol^{-1}). Therefore, the $^1O_2$ may be generated by two pathways: that is, in addition to the conventional pathway, by ET from T_1 (ET 1 in Fig. 5a and

equation (1)), the ET from S_1 to $^3O_2$ may also lead to $^1O_2$ generation during the S_1–T_1 intersystem crossing transition (ET 2 in Fig. 5a and equation (2)). Therefore, an overall $^1O_2$ quantum yield greater than 1.0 can be achieved[33,44].

$$T_1 + O_2\left(^3\sum_g^-\right) \rightarrow S_0 + O_2\left(^1\Delta_g\right) \quad (1)$$

$$S_1 + O_2\left(^3\sum_g^-\right) \rightarrow T_1 + O_2\left(^1\Delta_g\right) \quad (2)$$

To further verify the MSS mechanism,we measured the fluorescence intensity at 680 nm and the $^1O_2$ quantum yield of GQDs in solutions with different oxygen concentrations. Theoretically, in the MSS process, the $^1O_2$ yield (Q_Δ) can be expressed as a function of the oxygen-dependent fluorescence intensity, as described in equation (3)[44]

$$Q_\Delta = Q_{\Delta M} + k\frac{F}{F^0}, \quad (3)$$

where $Q_{\Delta M}$ is the maximum $^1O_2$ yield by ET from the S_1 and T_1 states, k is a coefficient related to the formation efficiency of T_1 and $^1O_2$ yields from S_1 and T_1 states, respectively, and F^0 and F are the fluorescence intensities of GQDs at 680 nm in the absence and presence of O_2, respectively. As illustrated in Fig. 5b, the fluorescence intensity of the GQD solution at 680 nm decreased linearly with the increase in the O_2 concentration in solution. Extrapolating the line produced the fluorescence intensity in the absence of O_2 (F^0): 907. On the basis of Fig. 5b, a linear dependence of Q_Δ on F/F^0 was plotted, as presented in Fig. 5c. The interception of the line with the Q_Δ axis yields a $Q_{\Delta M}$ of 1.4, which coincides very well with our experimental observations. The MSS process of GQD_S generating $^1O_2$ was thus further verified. The MSS mechanism proposed here also suggests that a $^1O_2$ quantum yield higher than 1.0 can be achieved only in the visible region (shorter than 636 nm, corresponding to the theoretical photo energy to drive the MSS for $^1O_2$ generation).

In summary, we have demonstrated an approach to prepare GQDs on a large scale using a simple hydrothermal method with polythiophenes as the precursors. The GQDs exhibit a combination of properties, including broad absorption from the visible to the NIR, deep-red emission, good aqueous dispersibility, high photo- and pH stability and favourable biocompatibility. More importantly, the GQDs exhibited a high $^1O_2$ generation yield, greater than 1.3 (approximately twice as high as that of all of the state-of-the-art PDT agents) via a new MSS process. The collective properties of the GQDs enable them to act as a multifunctional nanoplatform for the simultaneous imaging and highly efficient *in vivo* PDT of cancer. Although the high $^1O_2$ generation yield of GQDs was achieved only in the visible light region, there are important applications for medical treatment, such as PDT of skin cancers and tumours located near the skin. In these cases, a high $^1O_2$ quantum yield is favourable. Owing to their high $^1O_2$ generation efficiency, the GQDs can also be applied as efficient, environment friendly and visible-light-responsive photocatalysts for the degradation of persistent organic pollutants and microorganisms.

Methods

Synthesis of PT2. PT2 was synthesized as reported recently by our group[28], the synthetic rout can be detailed as follows and Supplementary Fig. 15. In brief, compoud **1** was abtained by nucleophilic addition with 4-Bromobenzyl bromide and *N*, *N*-dimethyldodecylamine in a mixed solvent ($CH_2Cl_2/CH_3OH = 3/2$) under N_2 protection. Then, compoud **1** via a suzuki reaction with thiophene-3-boronic acid catalysed by $Pd(PPh_3)_4$ leads to compoud **2**. Subsequently, PT2 was prepared via an oxidative polymerization with compoud **2** under nitrogen catalysed by $FeCl_3$ in anhydrous $CHCl_3$.

Synthesis of GQDs. The GQDs were prepared by hydrothermal treatment of polythiophene (PT2). In a typical synthesis, 30 mg of PT2 was dispersed in 40 ml of NaOH solution (0.5 mM). The mixture was treated ultrasonically for 30 min and then transferred into an autoclave and heated at 170 °C for a period of 24 h. After cooling to room temperature, the GQDs were collected by removing the large particles, through filtering using 0.22-μm membranes, and then dialysed against distilled water several times to remove the residual NaOH. The GQDs were dispersed in water for further characterization and use.

Molecular weight measurements. To calculate the molar concentration of the GQDs, we employed the gel permeation chromatography (GPC) method to evaluate their molecular weight, using polystyrene as the standard and N,N-dimethylformamide (DMF) as the eluent (GPC, Agilent 1100). The media molecular weight and weight-average molar mass (Mw) were 7.46×10^4 and 9.3×10^4 g mol^{-1}, respectively. The molecular weight used in the manuscript was 7.46×10^4 g mol^{-1}, the media molecular weight.

$^1O_2$ quantum yield measurements via the chemical method. Water-soluble Na_2-ADPA was used as the $^1O_2$-trapping agent, and RB was used as the standard photosensitizer. In the experiments, 60 μl of Na_2-ADPA solution (1 mg ml^{-1}) was added to 1.5 ml of GQD solution, and white light (400–800 nm) with a power density of 6.5 mW cm^{-2} was employed as the irradiation source. To eliminate the inner-filter effect, the absorption maxima of RB and the GQDs were adjusted to ~0.2 OD. The absorption of Na_2-ADPA at 378 nm was recorded at various irradiation times to obtain the decay rate of the photosensitizing process. The $^1O_2$ quantum yield of the GQDs in water (Φ_{GQDs}) was calculated using the following formula:

$$\Phi_{GQDs} = \Phi_{RB} * K_{GQDs} * A_{RB} / (K_{RB} * A_{GQDs}) \quad (4)$$

where K_{GQDs} and K_{RB} are the decomposition rate constants of Na_2-ADPA by the GQDs and RB, respectively. A_{GQDs} and A_{RB} represent the light absorbed by the GQDs and RB, respectively, which are determined by integration of the optical absorption bands in the wavelength range 400–700 nm. Φ_{RB} is the $^1O_2$ quantum yield of RB, and $\Phi_{RB} = 0.75$ in water.

For the $^1O_2$ quantum yield measurements at different pH values, the pH value of the GQD/Na_2-ADPA mixture solutions was adjusted to 6.0 and 8.0 using HCl and NaOH, respectively. For the fluorescence intensities and $^1O_2$ quantum yield measurements under different oxygen concentrations, the fluorescence intensities and quantum yields of $^1O_2$ of the GQD solutions were determined as a function of the dissolved oxygen concentration in the range from 1.8 to 8.5 p.p.m. The oxygen concentration was varied in the following manner: the GQD solutions were deoxygenated by three freeze-pump-thaw cycles and then replenished with pure oxygen. The final concentrations of oxygen were determined using a dissolved oxygen meter (Beijing Time power Measure and Control Equipment Co., Ltd). Before each measurement of the quantum yields of $^1O_2$ of the GQDs, the corresponding fluorescence spectra were detected to demarcate their fluorescence intensities, and then the $^1O_2$ quantum yields of the GQDs were measured using the chemical trapping method.

$^1O_2$ quantum yield measurements by detecting $^1O_2$ emission. The $^1O_2$ emission signals of the GQDs were detected in a HITACHI FL 900 fluorescence spectrophotometer with a 532-nm excitation laser and a NIR detector. Considering the short PL lifetime of $^1O_2$ in water, the GQD solution was lyophilized, and the solid power was dissolved in a 15:1 (v/v) CH_3CN-D_2O solution. The absorptions of RB and the GQDs at 532 nm were adjusted to ~0.2 OD. The $^1O_2$ quantum yield of the GQDs could be obtained using

$$\Phi_{GQDs} = \Phi_{RB} * I_{GQDs} / I_{RB} \quad (5)$$

where I_{GQDs} and I_{RB} represent the PL peak areas of $^1O_2$ produced by the GQDs and RB, respectively.

Photostability evaluation of GQDs. HeLa cells were obtained from the Peking Union Medical College. The HeLa cells were cultured in fresh media (DMEM/F12 supplemented with 10% fetal bovine serum, 50 unit ml^{-1} of penicillin, and 50 μg ml^{-1} of streptomycin) at 37 °C in a humidified incubator containing 5% CO_2. The HeLa cells were incubated with 40 μl of GQDs (1 mg ml^{-1}) or 40 μl of CdTe QDs (1 mg ml^{-1}) in 1 ml of culture medium for 60 min at 37 °C. Then, the cells were washed using PBS and fixed with 4% paraformaldehyde in PBS for 20 min. The fixed HeLa cells were carefully washed with PBS three times. These cells were then irradiated and imaged using a Nikon C1 laser-scanning confocal microscope. The windows for the GQDs and CdTe QDs were collected at 680–740 and 580–640 nm, respectively. The images were captured with a cooled CCD camera at 100-ms intervals for each colour automatically.

***In vitro* imaging and PDT.** In the *in vitro* imaging experiments, HeLa cells were incubated with 40 μl of GQDs (0.4 μM) in 1 ml of culture media at 37 °C. After incubating the mixtures for 1 h, the cells were washed with PBS twice to remove

non-specifically bound QDs. Images were also acquired with a Nikon C1si laser scanning confocal microscopy.

In the *in vitro* PDT experiments, HeLa cells were incubated with 20 µl of Hoechst 33342 (1.8 µM) for 20 min, and then 40 µl of GQDs (0.4 µM) were added to the culture medium for 1 h at 37 °C. The control experiments did not include GQDs. After the medium was removed, the cells were carefully washed twice with PBS. Then, the HeLa cells were continuously irradiated using 405 and 637 nm lasers equipped with scanning confocal microscopy. Images were captured with a cooled CCD camera at 100-ms intervals for each colour automatically.

To compare the dark toxicity and phototoxicity of the GQDs and PpIX QDs, the GQD stock solutions were diluted with fresh medium to various concentrations (0.036, 0.09 0.18, 0.36, 0.9 and 1.8 µM). The PpIX stock solutions were also diluted with fresh medium to various concentrations (0.36, 0.9, 1.8, 3.6, 9.0 and 18 µM). The cell medium was then exchanged for different concentrations of GQDs or PpIX medium solution. The cells were then incubated with these solutions at 37 °C in 5% CO_2 for 4 h, and the cultures were then irradiated using a 500-W Xe lamp as the light source with an intensity of 6.5 mW cm^{-2} for 0 or 10 min before removing the GQDs or PpIX solution and adding fresh medium. Subsequently, the plates were incubated at 37 °C in 5% CO_2 for 24 h. The cell medium solutions were exchanged for 100 µl of fresh medium, followed by the addition of 20 µl of MTT solution to each well. The culture plates were then incubated at 37 °C in 5% CO_2 for 4 h. The culture medium was discarded, and 100 µl of dimethylsulfoxide was added. The absorbance of an untreated cell population under the same experimental conditions was used as the reference point to establish 100% cell viability.

***In vivo* imaging and PDT.** Animal experiments were approved by the China Committee for Research and Animal Ethics in compliance with the law on experimental animals. All animal experiments were conducted at Anticancer Biotechnology (Beijing) Co. Ltd. For the *in vivo* imaging, female BALB/nu mice (6 weeks old, 18–20 g) received a subcutaneous injection of 20 µl (27 µM) GQD aqueous solution. The excitation wavelength was 502–540 nm, and the collected fluorescence channels were 695–775 nm. For the *in vivo* PDT treatment, female BALB/nu mice with subcutaneous breast cancer (MDA MB-231 green-fluorescent protein) xenografts were selected as the animal model. The *in vivo* fluorescence images were acquired using a FluorVivo Model-300.

Photothermal effect measurements. Photothermal effect data were acquired from Agilent 34970A using a T type thermocouple. White light (400–800 nm) was generated from a xenon light source (Solar-500). The intensity of the incident beam was determined by a radiometer (Photoelectric Instrument Factory of Beijing Normal University). To measure the photothermal conversion performance of the GQDs, 1.2 ml of GQD (13.5 or 27 µM) solution was introduced into a quartz cuvette and irradiated with white light (400–800 nm) at a power density of 80 mW cm^{-2} for 20 min. Pure water was used as a negative control. A thermocouple probe with an accuracy of 0.1 °C was inserted into the GQD aqueous solution perpendicular to the light path. The temperature was recorded at 1-s intervals by a digital thermometer with a thermocouple probe.

Sample characterizations. STEM and HRTEM images were recorded on a Cs-corrected Titan 80–300 microscope operated at 300 kV. X-ray diffraction patterns were obtained using an X-ray diffractometer (Bruker, Germany) with Cu-Kα radiation. The 2θ scanning range was 10° to 80° with a scanning speed of 0.1° s^{-1}. XPS was performed using an ESCALAB 250 spectrometer with Al Kα X-ray excitation (1,486.6 eV). Raman spectra were measured using an Invia-Reflex Raman system using a 785-nm laser. UV–vis and fluorescence spectra were obtained using Hitachi U-3010 and F-4500 spectrophotometers, respectively. ROS were detected using the ESR technique (ESP300E, Bruker).

References

1. Ferlay, J. *et al.* Estimates of worldwide burden of cancer in 2008: GLOBOCAN 2008. *Int. J. Cancer* **127,** 2893–2917 (2010).
2. Dolmans, E. J. G. J., Fukumura, D. & Jain, P. K. Photodynamic therapy for cancer. *Nat. Rev. Cancer* **3,** 380–387 (2003).
3. Castano, A. P., Mroz, P. & Hamblin, M. R. Photodynamic therapy and anti-tumor immunity. *Nat. Rev. Cancer* **6,** 535–545 (2006).
4. Moore, C. M., Pendse, D. & Emberton, M. Photodynamic therapy for prostate cancer-a review of current status and future promise. *Nat. Clin. Pract. Urol.* **6,** 18–30 (2009).
5. Lovell, J. F., Liu, T. W. B., Chen, J. & Zheng, G. Activatable photosensitizers for imaging and therapy. *Chem. Rev.* **110,** 2839–2857 (2010).
6. Detty, M. R., Gibson, S. L. & Wagner, S. J. Current clinical and preclinical photosensitizers for use in photodynamic therapy. *J. Med. Chem.* **47,** 3897–3915 (2004).
7. Huang, Z. A review of progress in clinical photodynamic therapy. *Technol. Cancer Res. Treat.* **4,** 283–293 (2005).
8. Gao, X. H., Cui, Y. Y., Levenson, R. M., Chung, L. W. K. & Nie, S. M. *In vivo* cancer targeting and imaging with semiconductor quantum dots. *Nat. Biotechnol.* **22,** 969–976 (2004).
9. Michalet, X. *et al.* Quantum dots for live cells, *in vivo* imaging, and diagnostics. *Science* **307,** 538–544 (2005).
10. Resch-Genger, U., Grabolle, M., Cavaliere-Jaricot, S., Nitschke, R. & Nann, T. Quantum dots versus organic dyes as fluorescent labels. *Nat. Mathods* **5,** 763–775 (2008).
11. Ye, L. *et al.* A pilot study in non-human primates shows no adverse response to intravenous injection of quantum dots. *Nat. Nanotech.* **7,** 453–458 (2012).
12. Bakalova, R., Ohba, H., Zhelev, Z., Ishikawa, M. & Baba, Y. Quantum dots as photosensitizers? *Nat. Biotechnol.* **22,** 1360–1361 (2004).
13. Idris, N. M. *et al. In vivo* photodynamic therapy using upconversion nanoparticles as remote-controlled nanotransducers. *Nat. Med.* **18,** 1580–1585 (2012).
14. Xiao, L., Gu, L., Howell, S. B. & Sailor, M. J. Porous silicon nanoparticle photosensitizers for singlet oxygen and their phototoxicity against cancer cells. *ACS Nano* **5,** 3651–3659 (2011).
15. Samia, A. C. S., Chen, X. B. & Burda, C. Semiconductor quantum dots for photodynamic therapy. *J. Am. Chem. Soc.* **125,** 15736–15737 (2003).
16. Tsay, J. M. *et al.* Singlet oxygen production by peptide-coated quantum dot-photosensitizer conjugates. *J. Am. Chem. Soc.* **129,** 6865–6871 (2007).
17. Geim, A. K. & Novoselov, K. S. The rise of graphene. *Nat. Mater.* **6,** 183–191 (2007).
18. Geim, A. K. Graphene: status and prospects. *Science* **324,** 1530–1534 (2009).
19. Novoselov, K. S. *et al.* A roadmap for graphene. *Nature* **490,** 192–200 (2012).
20. Kostarelos, K., Bianco, A. & Prato, M. Promises, facts and challenges for carbon nanotubes in imaging and therapeutics. *Nat. Nanotech.* **4,** 627–633 (2009).
21. Krishna, V., Stevens, N., Koopman, B. & Moudgil, B. Optical heating and rapid transformation of functionalized fullerenes. *Nat. Nanotech.* **5,** 330–334 (2010).
22. Xu, X. Y. *et al.* Electrophoretic analysis and purification of fluorescent single-walled carbon nanotube fragments. *J. Am. Chem. Soc.* **126,** 12736–12737 (2004).
23. Baker, S. N. & Baker, G. A. Luminescent carbon nanodots: Emergent nanolights. *Angew. Chem. Int. Ed.* **49,** 6726–6744 (2010).
24. Li, H. T. *et al.* Carbon nanodots: synthesis, properties and applications. *J. Mater. Chem.* **22,** 24230–24253 (2012).
25. Shen, J. H., Zhu, Y. H., Yang, X. L. & Li, C. Z. Graphene quantum dots: emergent nanolights for bioimaging, sensors, catalysis and photovoltaic devices. *Chem. Commun.* **48,** 3686–3699 (2012).
26. Huang, P. *et al.* Light-triggered theranostics based on photosensitizer conjugated carbon dots for simultaneous enhanced-fluorescence imaging and photodynamic therapy. *Adv. Mater.* **24,** 5104–5110 (2012).
27. Markovic, Z. M. *et al.* Graphene quantum dots as autophagy-inducing photodynamic agents. *Biomaterials* **33,** 7084–7092 (2012).
28. Lan, M. H. *et al.* Copolythiophene-derived colorimetric and fluorometric sensor for visually supersensitive determination of lipopolysaccharide. *J. Am. Chem. Soc.* **134,** 6685–6694 (2012).
29. Zhou, J. *et al.* An electrochemical avenue to blue luminescent nanocrystals from multiwalled carbon nanotubes (MWCNTs). *J. Am. Chem. Soc.* **129,** 744–745 (2007).
30. Dong, Y. Q. *et al.* Carbon-based dots co-doped with nitrogen and sulfur for high quantum yield and excitation-independent emission. *Angew. Chem. Int. Ed.* **52,** 7800–7804 (2013).
31. Liu, L. *et al.* Bottom-up fabrication of photoluminescent graphene quantum dots with uniform morphology. *J. Am. Chem. Soc.* **133,** 15221–15223 (2011).
32. López-Ríos, T., Sandré, É., Leclercq, S. & Sauvain, É. Polyacetylene in diamond films evidenced by surface enhanced Raman scattering. *Phy. Rev. Lett.* **76,** 4935–4938 (1996).
33. Kanner, R. C. & Foote, C. S. Singlet oxygen production from singlet and triplet states of 9, l0-Dicyanoanthracene. *J. Am. Chem. Soc.* **114,** 678–681 (1992).
34. Ye, R. Q. *et al.* Coal as an abundant source of graphene quantum dots. *Nat. Commun.* **4,** 2943–2948 (2013).
35. Zhang, Z. P., Zhang, J., Chen, N. & Qu, L. T. Graphene quantum dots: an emerging material for energy-related applications and beyond. *Energy Environ. Sci.* **5,** 8869–8890 (2012).
36. Li, L. L. *et al.* Focusing on luminescent graphene quantum dots: current status and future perspectives. *Nanoscale* **5,** 4015–4039 (2013).
37. Xing, C. F. *et al.* Design guidelines for conjugated polymers with light-activated anticancer activity. *Adv. Funct. Mater.* **21,** 4058–4067 (2011).
38. Gollnick, K. & Held, S. H. Hydroxyanthraquinones as sensitizers of singlet oxygen reactions: quantum yields of triplet formation and singlet oxygen generation in acetonitrile. *J. Photochem. Photobiol. A Chem.* **69,** 155–165 (1992).
39. Vankayala, R., Sagadevan, A., Vijayaraghavan, P., Kuo, C. L. & Hwang, K. C. Metal nanoparticles sensitize the formation of singlet oxygen. *Angew. Chem. Int. Ed.* **50,** 10640–10644 (2011).

40. Cao, L. *et al.* Carbon dots for multiphoton bioimaging. *J. Am. Chem. Soc.* **129,** 11318–11319 (2007).
41. Liu, Q. L. *et al.* Structural effect and mechanism of C_{70}-carboxyfullerenes as efficient sensitizers against cancer cells. *Small* **8,** 2070–2077 (2012).
42. Lovrić, J., Cho, S. J. & Winnik, F. M. Unmodified cadmium telluride quantum dots induce reactive oxygen species formation leading to multiple organelle damage and cell death. *Chem. Biol.* **12,** 1227–1234 (2005).
43. Chu, M. Q. *et al.* Laser light triggered-activated carbon nanosystem for cancer therapy. *Biomaterials* **34,** 1820–1832 (2013).
44. Schweitzer, C. & Schmidt, R. Physical mechanisms of generation and deactivation of singlet oxygen. *Chem. Rev.* **103,** 1685–1757 (2003).

Acknowledgements

This work was supported by the National Natural Science Foundation of China (Grant Nos. 61227008, 51172244, 11179006 and 21373250), the Key Research Program of the Chinese Academy of Sciences (Grant No. KGZD-EW-T02) and Research Grants Council of the Hong Kong Special Administrative Region, China (Project No. CityU102010). We thank Dr Zhongshan Deng from TIPC for the photothermal therapy experimental assistance, Professor Yi Li and Professor Xuesong Wang from TIPC for helpful discussions on the photophysical properties of GQDs.

Author contributions

P.W. planed and supervised the project. J.G., M.L., P.W. and W.Z. designed and carried out the detailed experiments, analysed the data and wrote the whole paper. B.Z., L.G. and H.Z. helped for the photodynamic therapy. W.L., H.W., Q.J. and G.N. contributed to the photophysical experiments. X.H. (TIPC), X.M. and X.H (BUT). contributed to the STEM and HRTEM measurements and analysis of the data. C-S.L. contributed to the XPS, Raman spectra measurements and discussion of the paper.

Additional information

Supplementary Information accompanies this paper at http://www.nature.com/naturecommunications

Competing financial interests: The authors declare no competing financial interests.

Reprints and permission information is available online at http://npg.nature.com/reprintsandpermissions/

How to cite this article: Ge, J. *et al.* A graphene quantum dot photodynamic therapy agent with high singlet oxygen generation. *Nat. Commun.* 5:4596 doi: 10.1038/ncomms5596 (2014).